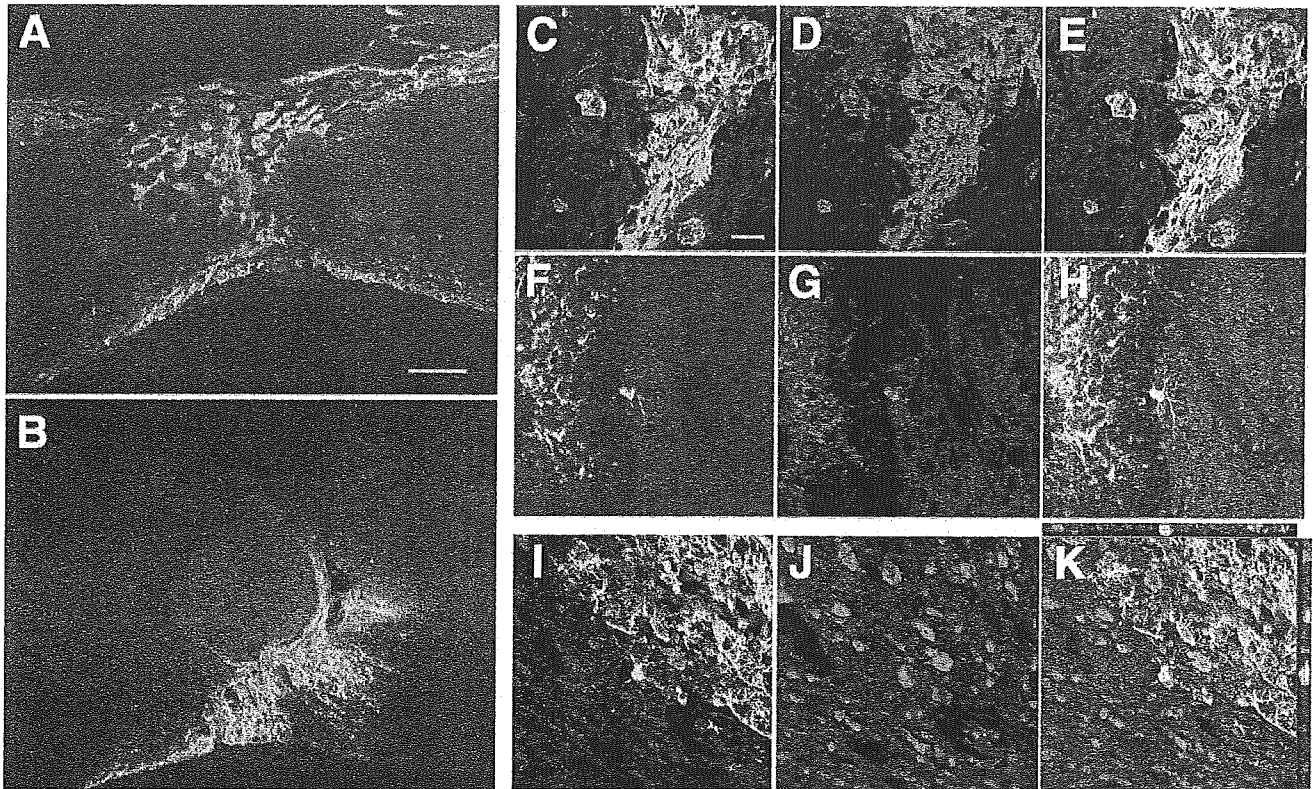
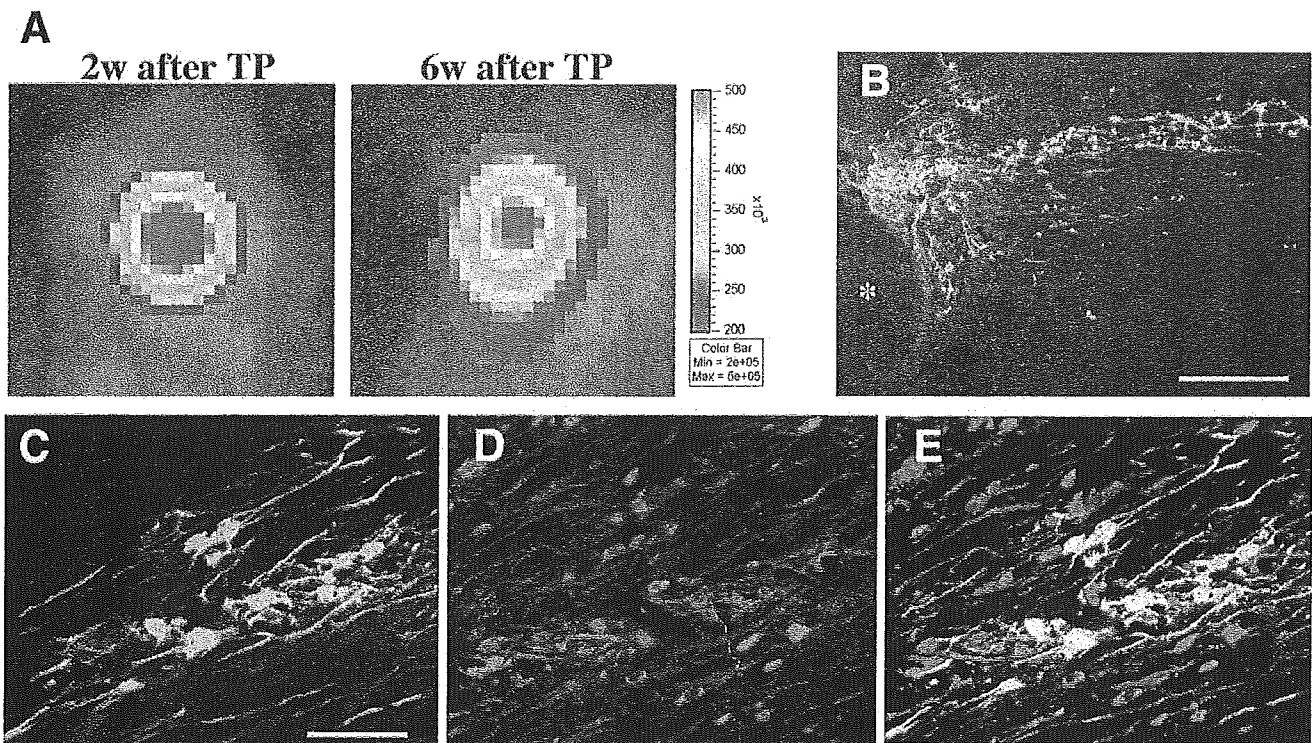


**Fig. 5**



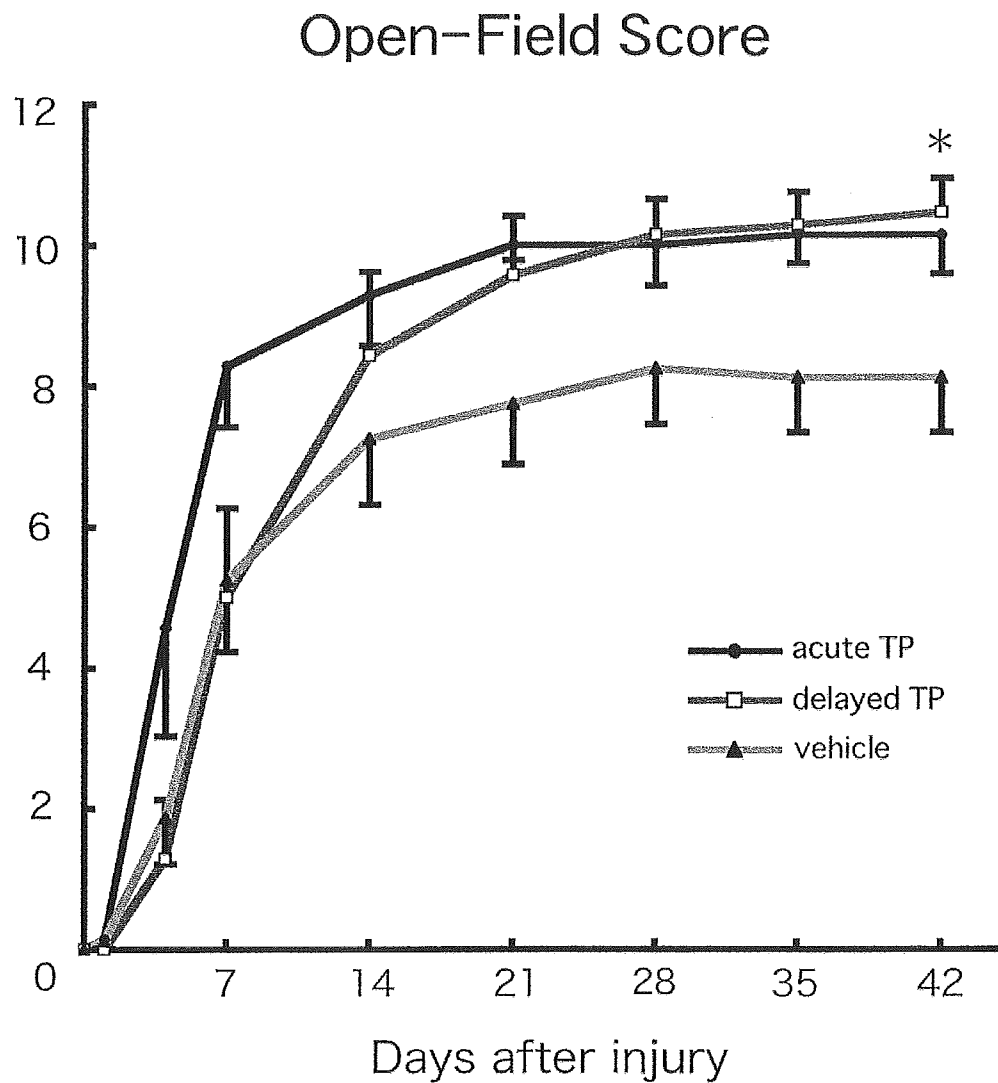
**Figure 5.** Transplanted NSPCs integrated and differentiated in the injured spinal cord at 6 wk after injury. Integrated cells were morphologically different between acute (**A**, **C–E**) and delayed (**B**, **F–K**) transplantation groups. A majority of transplanted NSPCs in the acute phase were immunoreactive for GFAP (**C–E**) and formed a glial scar at the lesion epicenter. In contrast, delayed transplanted NSPCs integrated around the scar tissue area, and a portion of these cells were identified as single cells differentiated into APC-positive oligodendrocytes with multiple myelin-forming processes (**F–H**) or Hu-positive neurons (**I–K**). Green represents GFP-positive NSPCs, and blue (**H**) represents Hoechst. **K**) Orthogonal view to confirm the double labeling with Hu and GFP. Scale bar: 200  $\mu\text{m}$  (**A**) and 25  $\mu\text{m}$  (**C**).

Fig. 6



**Figure 6.** Representative image of configuration shift in BLI and histology of migratory cells in delayed transplantation group. **A)** The signal configuration of grafted NSPCs, which was round at 2 wk after transplantation, became elliptical at 6 wk after transplantation. **B)** Histological analysis revealed integrated cells migrating away from the scar area at lesion epicenter (\*) in a caudal direction with extended neurites. The confocal image revealed that a portion of these cells were Hu-positive neurons (**C–E**). Scale bar: 200  $\mu\text{m}$  (**B**) and 50  $\mu\text{m}$  (**C**).

Fig. 7



**Figure 7.** Partial functional recovery of paraplegic mice by transplantation of NSPCs. Both acute and delayed transplantation (TP) of NSPCs promoted recovery of hindlimb movement compared with vehicle injection (vehicle). There was a statistically significant difference between the delayed TP group and the vehicle-treated group in BBB score at 6 wk after injury. Values are means  $\pm$  SE ( $n=8$ ); \* $P < 0.05$ .

## Comparison of Various Bone Marrow Fractions in the Ability to Participate in Vascular Remodeling After Mechanical Injury

MAKOTO SAHARA,<sup>a</sup> MASATAKA SATA,<sup>a,b,d</sup> YUMI MATSUZAKI,<sup>c,e</sup> KIMIE TANAKA,<sup>a</sup> TOSHIHIRO MORITA,<sup>a</sup>  
YASUNOBU HIRATA,<sup>a</sup> HIDEYUKI OKANO,<sup>c,e</sup> RYOZO NAGAI<sup>a</sup>

Departments of <sup>a</sup>Cardiovascular Medicine and <sup>b</sup>Advanced Clinical Science and Therapeutics, University of Tokyo Graduate School of Medicine, Tokyo, Japan; <sup>c</sup>Department of Physiology, Keio University School of Medicine, Tokyo, Japan;

<sup>d</sup>PRESTO, Japan Science and Technology Agency, Kawaguchi, Saitama, Japan;

<sup>e</sup>CREST, Japan Science and Technology Agency, Kawaguchi, Saitama, Japan

**Key Words.** Endothelial cells • Hematopoietic stem cells • Progenitor • Smooth muscle cells • Transdifferentiation

### ABSTRACT

In contrast to conventional assumption, recent reports propose the possibility that hematopoietic stem cells (HSCs) may have broader potential to differentiate into various cell types. Here, we tested the pluripotency of HSCs by comparing vascular lesions induced by mechanical injury after bone marrow reconstitution with total bone marrow (TBM) cells, c-Kit<sup>+</sup> Sca-1<sup>+</sup> Lin<sup>-</sup> (KSL) cells, or a single HSC cell (Tip-SP CD34<sup>-</sup> KSL cell, CD34<sup>-</sup> c-Kit<sup>+</sup> Sca-1<sup>+</sup> Lin<sup>-</sup> cell with the strongest dye-efflux activity) harboring green fluorescent protein (GFP).

The lesions contained a significant number of GFP-positive cells in the TBM and KSL groups, whereas GFP-positive cells were rarely detected in the HSC group. These results suggest that transdifferentiation of a highly purified HSC seems to be a rare event, if it occurs at all, whereas bone marrow cells including the KSL fraction can give rise to vascular cells that substantially contribute to repair or lesion formation after mechanical injury. STEM CELLS 2005;23:874–878

### INTRODUCTION

Recent evidence suggests that bone marrow-derived cells may participate in regeneration of remote organs [1]. Bone marrow contains both hematopoietic and nonhematopoietic cells. Hematopoietic stem cells (HSCs) are defined as having the capacity for self-renewal and the ability to differentiate into all mature hematopoietic lineages [2]. Although it was assumed that HSCs give rise to hematopoietic cells, recent reports proposed the possibility that HSCs may have the broader potential to differentiate into nonhematopoietic cells, including epithelial cells [3], hepatocytes [4, 5], cardiomyocytes [6], and vascular cells [7]. In contrast, others cast doubt on the pluripotency of adult HSCs under physiological conditions by analyzing uninjured organs of bone marrow chimeric mice [8].

There might be two possibilities that account for the discrepancy. First, the HSCs used differ in their purity [4, 7, 8]. Most of the studies analyzed the CD34<sup>-</sup>, c-Kit<sup>+</sup>, Sca-1<sup>+</sup>, Lineage<sup>-</sup> (CD34<sup>-</sup> KSL) bone marrow cells [4, 7], which have been assumed as the most primitive HSCs [9]. However, even in the best case series reported [9], only one in five recipients showed successful engraftment after single-cell transplantation, indicating that the CD34<sup>-</sup> KSL fraction represents a heterogeneous population containing nonhematopoietic cells. It is possible that nonhematopoietic cells among the CD34<sup>-</sup> KSL cells might be responsible for the pluripotency. Second, the apparent discrepancy could merely derive from the analysis of noninjured versus injured tissues [10]. We reported that the mode of injury is crucial for the recruitment

Correspondence: Masataka Sata, M.D., Department of Cardiovascular Medicine, University of Tokyo Graduate School of Medicine, 7-3-1 Hongo, Bunkyo-ku, Tokyo 113-8655, Japan. Telephone: 81-3-3815-5411; Fax: 81-3-3814-0021; e-mail: msata-circ@umin.ac.jp Received January 11, 2005; accepted for publication May 19, 2005; first published online in STEM CELLS EXPRESS June 7, 2005. ©AlphaMed Press 1066-5099/2005/\$12.00/0 doi: 10.1634/stemcells.2005-0012

STEM CELLS 2005;23:874–878 www.StemCells.com

of bone marrow–derived cells to vascular remodeling [11]. Thus, it remains unclear whether a highly purified single HSC can contribute to vascular remodeling after severe vascular injuries, which are essential for bone marrow–derived cells to participate in vascular remodeling.

Here, we transplanted either total bone marrow (TBM) cells, KSL fraction cells, or a highly purified HSC into lethally irradiated wild-type mice [2]. In all groups, peripheral blood cells were successfully reconstituted. However, bone marrow–derived cells were seldom detected in the injured artery when a single HSC was injected into irradiated mice. These results suggest that it is a rare property for a purified HSC to transdifferentiate into vascular cells.

## MATERIALS AND METHODS

### Animals

All wild-type mice were purchased from SLC (Shizuoka, Japan). Transgenic mice (C57BL/6 background) that ubiquitously express enhanced green fluorescent protein (GFP) were described in previous reports [2, 7]. All procedures involving experimental animals were performed in accordance with protocols approved by the institutional committee for animal research of the University of Tokyo and complied with National Institutes of Health guidelines.

### Preparation of TBM Cells, KSL Cells, and a Highly Purified HSC

TBM cells were harvested from femora and tibias of the GFP-transgenic mice as previously described [7]. c-Kit<sup>+</sup>, Sca-1<sup>+</sup>, Lineage<sup>-</sup> fraction of bone marrow cells (KSL cells) were purified as described [7]. Briefly, TBM cells were stained with a cocktail of biotinylated monoclonal antibodies against lineage markers (B220/CD45R, clone RA3-6B2; Mac-1, clone M1/70; Gr-1, clone RB6-8C5; Thy1.2, clone 53-2.1; CD3, clone 145-2C11; CD4, clone GK1.5; CD8, clone 53-6.72; and TER 119, clone Ly-76; Pharmingen, San Diego, <http://wwwbdbiosciences.com/pharmingen>) for 20 minutes at 4°C. The cells were treated with streptavidin-conjugated immunomagnetic beads (BioMag; Polysciences, Inc., Warrington, PA, <http://www.polysciences.com/shop>) for 30 minutes to remove highly lineage-positive cells. The remaining cells were collected and stained with a phycoerythrin (PE)–conjugated anti-Sca-1 antibody (Pharmingen), an allophycocyanin-conjugated anti-c-Kit antibody (Pharmingen), and PE Texas red–conjugated streptavidin (Pharmingen) for 20 minutes at 4°C. KSL cells were purified by fluorescence-activated cell sorting (ALTRA; Beckman-Coulter, Tokyo, <http://www.beckmancoulter.com>). The bone marrow cells that had the strongest dye-efflux activity (Tip–side population [SP] cells) with a phenotype of CD34<sup>-</sup> c-Kit<sup>+</sup> Sca-1<sup>+</sup> Lineage<sup>-</sup> (CD34<sup>-</sup>KSL) were isolated as described [2]. A single-cell transplantation analysis has revealed that the Tip-SP CD34<sup>-</sup>KSL cells represent the most

primitive hematopoietic stem cells, with nearly complete hematopoietic engraftment activity [2].

### Stem Cell Transplantation

After lethal irradiation of 10.5 Gy (MBR-1520RB; Hitachi, Tokyo, <http://www.hitachi.com>),  $1 \times 10^6$  TBM cells (TBM group),  $3 \times 10^3$  KSL cells (KSL group), or a single Tip-SP CD34<sup>-</sup>KSL cell (HSC group) from GFP-transgenic mice were suspended in 0.3 ml phosphate-buffered saline and injected intravenously by tail vein puncture into C57BL/6 mice. The sites of intravenous injection, that is, tail vein or retro-orbital plexus, had no effect on the level of reconstitution (Y. Matsuzaki and H. Nakauchi, unpublished observations). The single Tip-SP CD34<sup>-</sup>KSL cell was transplanted with  $2 \times 10^5$  TBM cells from C57BL/6 mice for radioprotection. Eight to 16 weeks after transplantation, peripheral blood samples were collected from the retro-orbital venous plexus. After erythrocytes were lysed with ACK lysing buffer (0.155 M ammonium chloride, 0.1 M disodium EDTA, and 0.01 M potassium bicarbonate) [12], cell suspensions were analyzed by flow cytometry to measure GFP signal (XL; Beckman-Coulter).

### Wire-Mediated Endovascular Injury and Histological Analysis

At 12 weeks after irradiation and stem cell transplantation, an endovascular arterial injury was induced to the femoral artery of the bone marrow chimeric mice by inserting a large wire (0.38 mm in diameter, No. C-SF-15-15 [Cook, Bloomington, IN, <http://www.cookgroup.com/profile/med-mfg/index.html>]) as described [7, 11, 13]. At 4 weeks, the injured femoral arteries were excised and fixed in 4% paraformaldehyde. To preserve GFP signal for histological analyses, the arteries were embedded in plastic resin (Technovit 8100; Heraeus Kulzer, Wehrheim, Germany, <http://www.heraeus-kulzer-us.com>) as described. Immunofluorescence doublestaining was performed as described elsewhere [7]. The plastic-embedded sections were incubated with primary antibodies (Cy3-conjugated anti- $\alpha$ -smooth muscle actin [ $\alpha$ -SMA], clone 1A4 [Sigma, St. Louis, <http://www.sigmaldrich.com>]; anti-CD31, clone MEC13.3 [BD Biosciences, San Jose, CA, <http://wwwbdbiosciences.com/index.shtml>]; anti-pan-endothelial cell antigen, clone MECA-32 [BD Biosciences]; anti-CD45, clone 30-F11 [BD Biosciences]) followed by incubation with Cy3-conjugated secondary antibodies (Jackson ImmunoResearch, West Grove, PA, <http://www.jacksonimmuno.com>). Nuclei were counterstained with Hoechst 33258 (Sigma). The sections were mounted with the ProLong Antifade Kit (Molecular Probes, Eugene, OR, <http://probes.invitrogen.com>) and observed under confocal microscopes (FLUOVIEW FV300; Olympus, Tokyo, <http://www.olympus-global.com/en/global>). Cell number was counted in the neointima and media of a cross-section of each artery [7, 11]. Frequency of GFP-positive cells among total cells is reported.

### Statistics

The results are presented as the mean  $\pm$  SE of the mean. Comparisons among the three groups were evaluated by one-way analysis of variance followed by Scheffe's post hoc test. Statistical significance was defined as  $p < .05$ .

## RESULTS

### Significant Engraftment of a Single Tip-SP CD34-KSL Cell

Either TBM cells ( $1 \times 10^6$ , TBM group), c-Kit<sup>+</sup>, Sca-1<sup>+</sup>, Lin<sup>-</sup> cells ( $3 \times 10^3$ , KSL fraction), or a single Tip-SP CD34-KSL cell (1, HSC fraction) were injected into lethally irradiated wild-type mice. Consistent with our previous report [2], a single Tip-SP CD34-KSL cell showed significant donor cell engraftment for long term (Figs. 1A, 1B). Consistent with our previous study [2], both myelocytes/monocytes and T/B lymphocytes derived from a single Tip-SP cell were detected at 3, 6, and 12 months after transplantation. Flow cytometry at 16 weeks after bone marrow reconstitution revealed that peripheral blood cells had been reconstituted with the injected cells in TBM ( $79.6\% \pm 5.1\%$ ), KSL ( $68.4\% \pm 5.1\%$ ), and HSC ( $34.4\% \pm 6.5\%$ ) groups (Fig. 1B).

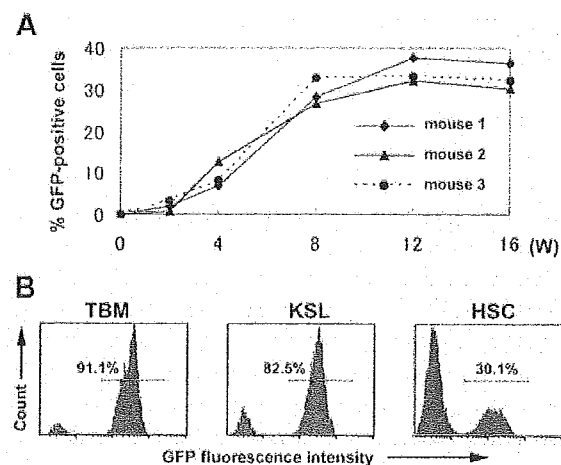


**Figure 1.** Successful engraftment of a single Tip-SP CD34-KSL cell,  $1 \times 10^6$  total bone marrow (TBM group) cells ( $n = 4$ ),  $3 \times 10^3$  c-Kit<sup>+</sup> Sca-1<sup>+</sup> Lin<sup>-</sup> (KSL group) fraction cells ( $n = 6$ ), or a single Tip-SP CD34-KSL cell (HSC group) ( $n = 7$ ) harboring green fluorescent protein (GFP) were injected into lethally irradiated wild-type mice. (A): Proportion of the GFP-positive cells in peripheral blood after transplantation of a single Tip-SP CD34-KSL cell. Time courses of three representative mice are reported. (B): Representative flow cytometric histograms of peripheral leukocytes in TBM, KSL, and HSC groups at 16 weeks after transplantation. Abbreviations: HSC, hematopoietic stem cell; SP, side population.

### Failure of a Single HSC-Derived Cell to Participate in Vascular Remodeling

Wire-mediated endovascular injury was induced to the femoral artery at 12 weeks after irradiation and injection. At 16 weeks after stem cell transplantation, the femoral arteries showed neointimal formation that mainly consisted of  $\alpha$ -SMA-positive cells in all groups (Fig. 2A). The neointima contained a significant number of GFP-positive cells in the TBM group ( $24.0\% \pm 7.2\%$ ;  $n = 4$ ) and the KSL group ( $14.1\% \pm 6.1\%$ ;  $n = 6$ ). On the other hand, GFP-positive cells were seldom detected in the neointima of the HSC group ( $0.2\% \pm 0.1\%$ ;  $n = 7$ ). Similarly, the media contained a significant number of GFP-positive cells in the TBM group ( $31.1\% \pm 11.2\%$ ) and KSL group ( $16.8\% \pm 6.6\%$ ). In contrast, GFP-positive cells were rarely detected in the media in the HSC group ( $2.7\% \pm 1.0\%$ ) (Fig. 2B, Table 1).

Next, we characterized the bone marrow-derived cells observed in the vascular lesions. In the KSL group as well as in the TBM group, many GFP-positive cells expressed  $\alpha$ -SMA in the neointima and media (Figs. 3A–3C). The bone marrow-derived cells on the luminal side were positive for endothelial markers (BS-lectin and CD31) (Figs. 3D, 3E), as previously reported [7]. In the HSC group, very few GFP-positive cells were detected in the lesions in the HSC group (Fig. 3C). All of the GFP-positive cells were positive for CD45 (Fig. 3F). We could not find GFP-positive cells that expressed  $\alpha$ -SMA or endothelial markers.

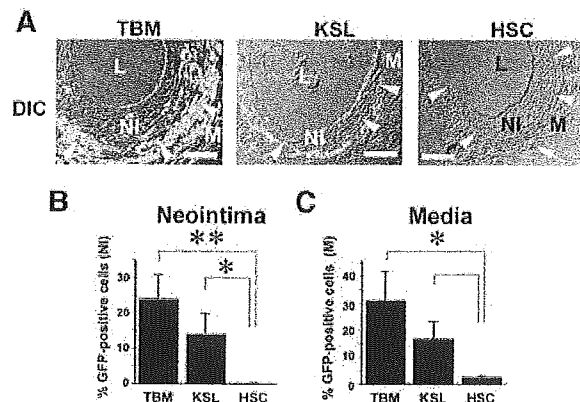


**Figure 2.** Failure of a highly purified HSC to contribute to vascular remodeling after mechanical vascular injury. (A): Representative cross-sections of the vascular lesions. At 12 weeks after irradiation and stem cell transplantation, wire-mediated injury was induced in the femoral artery of the bone marrow chimeric mice. The injured arteries were harvested at 16 weeks, embedded in plastic resin, and observed under a confocal microscope (FLUOVIEW FV300; Olympus). Arrowheads indicate the internal elastic lamina. Arrow indicates a GFP-positive cell observed in adventitia in the HSC group. Bar = 50  $\mu$ m. (B, C): Frequency of GFP-positive cells among the total cells in the (B) neointima and (C) media. \* $p < .05$ ; \*\* $p < .01$ . Abbreviations: DIC, differential interference contrast; GFP, green fluorescent protein; HSC, hematopoietic stem cell; KSL, c-Kit<sup>+</sup>, Sca-1<sup>+</sup>, Lin<sup>-</sup>; L, lumen; M, media; NI, neointima; TBM, total bone marrow.

**Table 1.** Frequency of green fluorescent protein (GFP)-positive cells in neointima and media per a cross-section 4 weeks after vascular injury in bone marrow chimeric mice

	Neointima	Media
	No. of GFP <sup>+</sup> cells/ no. of total cells per a cross-section	No. of GFP <sup>+</sup> cells/ no. of total cells per a cross-section
<b>TBM group</b>		
Mouse 1	162/406	48/81
Mouse 2	17/237	10/51
Mouse 3	104/339	45/120
Mouse 4	42/231	11/138
<b>KSL group</b>		
Mouse 1	89/209	22/53
Mouse 2	19/109	15/46
Mouse 3	4/150	3/69
Mouse 4	7/58	2/104
Mouse 5	10/145	14/133
Mouse 6	10/319	5/49
<b>HSC group</b>		
Mouse 1	0/291	1/44
Mouse 2	0/73	1/13
Mouse 3	0/210	1/24
Mouse 4	0/362	0/24
Mouse 5	0/235	0/68
Mouse 6	1/162	1/37
Mouse 7	1/104	1/42

Wire-mediated endovascular injury was induced in the femoral arteries of marrow chimeric mice, which received either total bone marrow cells ( $1 \times 10^6$ , TBM group), c-Kit<sup>+</sup>, Sca-1<sup>+</sup>, Lineage<sup>-</sup> cells ( $3 \times 10^5$ , KSL group), or highly purified hematopoietic stem cell (1, HSC group). The injured arteries were harvested 4 weeks after vascular injury and embedded in plastic resin. After counterstaining with Hoechst 33258, sections were observed under a fluorescence microscope. Cell number was counted in the neointima and media of a cross-section of each artery.

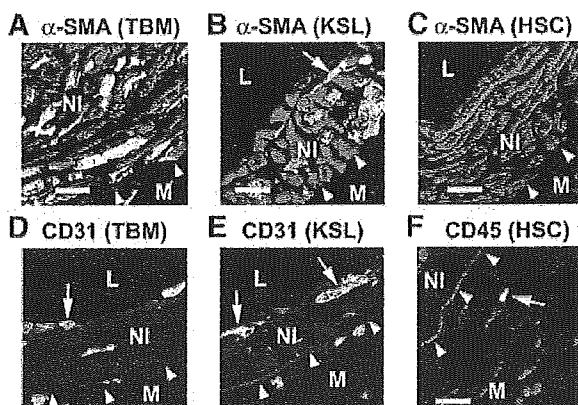


**Figure 3.** Double immunofluorescent images of the injured arteries. Plastic-embedded sections were stained for (A, B, C)  $\alpha$ -smooth muscle actin ( $\alpha$ -SMA, red), (D, E) CD31 (red), and (F) CD45 (red) followed by counterstaining with Hoechst 33258 (blue). Arrowheads indicate the internal elastic lamina. Arrows indicate green fluorescent protein-positive cells that were positive for markers. Bar = 10  $\mu$ m. Abbreviations: HSC, hematopoietic stem cell; KSL, c-Kit<sup>+</sup>, Sca-1<sup>+</sup>, Lineage<sup>-</sup>; L, lumen; M, media; NI, neointima; TBM, total bone marrow.

## DISCUSSION

The present study was designed to rigorously determine the plasticity of an HSC in vivo by analyzing the vascular lesions induced by wire injury after bone marrow reconstitution with a single HSC. Although a single HSC showed an appreciable level of hematopoietic engraftment activity, very few cells in the lesion were derived from the single HSC. In contrast, the GFP-positive cells substantially contributed to vascular remodeling when bone marrow was reconstituted with TBM cells or KSL cells [7, 11].

The HSCs used in this study had the strongest dye-efflux activity with nearly complete level of hematopoietic engraftment activity [2]. We could detect the single Tip-SP CD34-KSL-derived cells not only in T/B lymphocytes but also in myeloid lineage even at 12 months after transplantation [2]. Given the short life of mature myeloid cells, the long-term chimerism in total hematopoietic cells supports the notion that the single Tip-SP CD34-KSL cell undergoes self-renewal and continuously gives rise to progenitors of T/B lymphocytes and myelocytes/monocytes. Moreover, the Tip-SP CD34-KSL cells are homogenous in size and morphology as determined by flow cytometric analysis of 10,000 Tip-SP CD34-KSL cells [2]. About 90% of the Tip-SP CD34-KSL cells can form huge colonies in colony assay (Y. Matsuzaki, unpublished observations). We assume that the diverse chimerism results from the difference in place where the transplanted Tip-SP CD34-KSL cell homes.

Our result suggests that it is rare for a highly purified HSC to transdifferentiate into vascular cells. In contrast, the KSL fraction of bone marrow cells contained a distinct population that could substantially contribute to lesion formation. Although the KSL fraction is considered to be enriched in HSCs [4], mesenchymal stem cells or multipotent cells that are more primitive than HSCs [14] could be included in this fraction. It is plausible that those nonhematopoietic cells in the KSL fraction might be responsible for the KSL-derived endothelial-like cells or smooth muscle-like cells observed in the vascular lesion.

Recent reports suggest that HSCs adopt tissue-specific phenotype by cell fusion but not by transdifferentiation [15]. Previous reports documented polyploidization of vascular smooth muscle cells in response to mechanical and humoral stimuli [16]. Thus, it is possible that cell fusion can account for, at least in part, the accumulation of bone marrow-derived smooth muscle-like cells in vascular lesions. However, we seldom detected the HSC-derived cells in the vascular lesions. It would be rare for an HSC to contribute to vascular remodeling even by cell fusion.

## CONCLUSION

Our finding suggests that a highly purified murine HSC seldom transdifferentiates into vascular cells. Distinct cell populations other than hematopoietic cells may be responsible for most bone marrow-derived smooth muscle-like cells and endothelial like-cells that could be observed in vascular lesions after mechanical injury.

**ACKNOWLEDGMENTS**

This study was supported in part by grants from the Japanese

Ministry of Education, Culture, Sports, Science, and Technology and from the Japanese Ministry of Health, Labor, and Welfare.

**REFERENCES**

- 1 Poulos R, Alison MR, Forbes SJ et al. Adult stem cell plasticity. *J Pathol* 2002;197:441–456.
- 2 Matsuzaki Y, Kinjo K, Mulligan RC et al. Unexpectedly efficient homing capacity of purified murine hematopoietic stem cells. *Immunity* 2004;20:87–93.
- 3 Krause DS, Theise ND, Collector MI et al. Multi-organ, multi-lineage engraftment by a single bone marrow-derived stem cell. *Cell* 2001;105:369–377.
- 4 Lagasse E, Connors H, Al-Dhalimy M et al. Purified hematopoietic stem cells can differentiate into hepatocytes in vivo. *Nat Med* 2000;6:1229–1234.
- 5 Jang YY, Collector MI, Baylin SB et al. Hematopoietic stem cells convert into liver cells within days without fusion. *Nat Cell Biol* 2004;6:532–539.
- 6 Orlic D, Kajstura J, Chimenti S et al. Bone marrow cells regenerate infarcted myocardium. *Nature* 2001;410:701–705.
- 7 Sata M, Saiura A, Kunisato A et al. Hematopoietic stem cells differentiate into vascular cells that participate in the pathogenesis of atherosclerosis. *Nat Med* 2002;8:403–409.
- 8 Wagers AJ, Sherwood RI, Christensen JL et al. Little evidence for developmental plasticity of adult hematopoietic stem cells. *Science* 2002;297:2256–2259.
- 9 Osawa M, Hanada K, Hamada H et al. Long-term lymphohematopoietic reconstitution by a single CD34-low/negative hematopoietic stem cell. *Science* 1996;273:242–245.
- 10 Blau H, Brazelton T, Keshet G et al. Something in the eye of the beholder. *Science* 2002;298:361–362.
- 11 Tanaka K, Sata M, Hirata Y et al. Diverse contribution of bone marrow cells to neointimal hyperplasia after mechanical vascular injuries. *Circ Res* 2003;93:783–790.
- 12 Okada S, Yoshida T, Hong Z et al. Impairment of B lymphopoiesis in precocious aging (klotho) mice. *Int Immunol* 2000;12:861–871.
- 13 Sata M, Maejima Y, Adachi F et al. A mouse model of vascular injury that induces rapid onset of medial cell apoptosis followed by reproducible neointimal hyperplasia. *J Mol Cell Cardiol* 2000;32:2097–2104.
- 14 Jiang Y, Jahagirdar BN, Reinhardt RL et al. Pluripotency of mesenchymal stem cells derived from adult marrow. *Nature* 2002;418:41–49.
- 15 Vassilopoulos G, Wang PR, Russell DW. Transplanted bone marrow regenerates liver by cell fusion. *Nature* 2003;422:901–904.
- 16 Campbell JH, Tachas G, Black MJ et al. Molecular biology of vascular hypertrophy. *Basic Res Cardiol* 1991;86:3–11.



# Expression of a candidate marker for progenitor cells, Musashi-1, in the proliferative regions of human antrum and its decreased expression in intestinal metaplasia

Y Akasaka, Y Saikawa,<sup>1</sup> K Fujita, T Kubota,<sup>1</sup> Y Ishikawa, A Fujimoto, T Ishii, H Okano<sup>2</sup> & M Kitajima<sup>1</sup>

Department of Pathology, School of Medicine, Toho University, <sup>1</sup>Department of Surgery and <sup>2</sup>Department of Physiology, Keio University School of Medicine, Tokyo, Japan

Date of submission 11 December 2004  
Accepted for publication 15 March 2005

---

Akasaka Y, Saikawa Y, Fujita K, Kubota T, Ishikawa Y, Fujimoto A, Ishii T, Okano H & Kitajima M (2005) *Histopathology* 47, 348–356

## Expression of a candidate marker for progenitor cells, Musashi-1, in the proliferative regions of human antrum and its decreased expression in intestinal metaplasia

**Aim:** Reliable makers for progenitor cells in the human stomach have not been elucidated. The aim of the present study was to clarify whether Musashi-1 (Msi-1), which has recently been proposed as a stem cell marker in mouse intestine, serves as a marker for progenitor cells in human stomach.

**Methods and results:** Immunohistochemistry revealed that Msi-1+ cells were detected especially in the isthmus/neck region (the putative position of stem cells) of the adult antrum, but were limited to the basal regions of fetal pyloric glands during the early stages of development. These results suggest that Msi-1 expression occurs specifically in the stem cell-containing regions. Msi-1+ cells were intermingled

with proliferating cell nuclear antigen (PCNA)+ cells in the isthmus/neck region of the adult antrum, but did not coexpress PCNA or Ki67. Msi-1 expression overlapped partly with expression of MUC5AC and MUC6, indicating that Msi-1+ cells retain some features of both foveolar and pyloric gland cell differentiation phenotypes. In contrast, Msi-1 expression in gastric glands showing intestinal metaplasia (IM) became weaker than that in the glands without IM.

**Conclusion:** The specific expression of Msi-1 within the proliferative regions suggests that Msi-1 is a marker of cells with progenitor characteristics before active proliferation in human antrum.

**Keywords:** gastric-type mucins, Msi-1, progenitor cell, proliferation, stomach

**Abbreviations:** H&E, haematoxylin and eosin; IM, intestinal metaplasia; Msi-1, Musashi-1; PBS, phosphate-buffered saline; PCNA, proliferating cell nuclear antigen; SDS, sodium dodecyl sulphate; TBS, Tris-buffered saline

---

## Introduction

The epithelium of the adult stomach possesses a cell renewal system in which stem cells, thought to be present in the proliferative region of the isthmus/neck of the glands, differentiate into the surface mucous epithelial and glandular cells.<sup>1–6</sup> During this process, the immediate descendants derived from the stem cells

undergo a complex bipolar migration from the neck/isthmus region, moving either upward or downward.<sup>7,8</sup> Indeed, in the mouse stomach, all three types of progenitor cells (prepit, preneck, and preparietal cells) have been found to originate from multipotential granule-free cells in the isthmus region.<sup>9</sup> However, the lack of useful markers has made it difficult to characterize the progenitor cells in the human stomach and has hindered the study of their origin.<sup>10</sup>

The Musashi family is an evolutionarily conserved group of neural RNA-binding proteins that has representatives in *Drosophila melanogaster*, mice and humans.<sup>11–13</sup> The mammalian homolog, Musashi-1

Address for correspondence: Yoshikiyo Akasaka, Department of Pathology, School of Medicine, Toho University, 5-21-16 Omori-nishi, Ohta City, Tokyo 143-8540, Japan.  
e-mail: akasakay@med.toho-u.ac.jp

(Msi-1), is selectively expressed in neural progenitor cells, including neural stem cells.<sup>14</sup> Although its precise functions have not yet been clarified, Msi-1 is thought to be involved in the early asymmetric divisions that generate differentiated cells from neural stem cells. Interestingly, Msi-1 expression has also been identified outside the nervous system.<sup>15,16</sup> Specifically, it has been shown that Msi-1 is preferentially expressed in the predicted stem cell regions of murine and human intestinal crypts, suggesting that Msi-1 may be a marker for intestinal stem cells and their immediate descendants.<sup>15,16</sup> By analogy, stem cells are presumed to exist in human gastric glands and therefore it would be expected that Msi-1 is expressed in the glands.<sup>4,10</sup> In the present study, to clarify whether Msi-1 is expressed in the putative stem cells or progenitor cells in human gastric glands as in the murine intestine, we examined the expression profile of Msi-1 in the normal human stomach and compared it with those of proliferative antigens [proliferating cell nuclear antigen (PCNA) and Ki67] and gastric-type mucins (MUC5AC and MUC6).

## Materials and methods

### TISSUE SAMPLES

Thirty-three surgically resected non-cancerous gastric specimens were selected from the archives of the Department of Pathology, Hiratsuka City Hospital, Kanagawa, Japan. These had originally been obtained from 33 patients (aged 40–68 years) during surgery for duodenal ulcers or pancreatic tumours.

The fetal stomach was studied using gastric specimens removed at autopsy from two fetuses in the 14th week of gestation, two in the 19th week, three in the 22nd week, and three in the 27th week. Only well-preserved gastric specimens were used.

To examine the levels of Msi-1 expression in intestinal metaplasia (IM), 62 human stomach tissue samples were selected from biopsy specimens of IM mucosa (31 of incomplete IM type and 31 of complete IM type) from 62 patients (aged 36–72 years) at the Toho University School of Medicine. After a section from each sample was stained with haematoxylin and eosin (H&E), IM was classified as complete or incomplete according to previously described histological criteria: tissue of the complete type contains goblet cells and Paneth cells, whereas tissue of the incomplete type is devoid of Paneth cells.<sup>17</sup> Fully informed consent was obtained from all the adult subjects and the parents of the fetuses. All human materials examined in this study were treated in accordance with the guidelines of the Helsinki Declaration of 1975, as revised in 1983.

### IMMUNOHISTOCHEMISTRY

The Msi-1 antibody that we used (14H1) is a rat monoclonal antibody that recognizes amino acids 235–244 of Msi-1.<sup>14</sup> This region is conserved in *Xenopus*, mouse and human. The antibody does not cross-react with a related protein, Musashi-2.<sup>16</sup> Immunostaining for Msi-1 was performed as described previously.<sup>18</sup> In brief, the sections were treated with 3% H<sub>2</sub>O<sub>2</sub> in 0.1 M phosphate-buffered saline (PBS) for 10 min, then incubated with the Msi-1 antibody (diluted to a final concentration of 1 µg/ml) at 4°C overnight.<sup>14</sup> After incubation with a biotinylated goat anti-rat antibody (Dako, Glostrup, Denmark) for 1 h, the sections were washed with PBS and further incubated with streptavidin–biotin–peroxidase complex (Dako) for 40 min. The reaction products were stained with a 0.02% solution of 3,3'-diaminobenzidine in 0.05 M Tris–HCl buffer (pH 7.2) containing 0.01% H<sub>2</sub>O<sub>2</sub>. Slides were counterstained with haematoxylin, dehydrated and mounted. The negative control was incubated with an immunoglobulin from rat at the same final concentration, but without the primary antibody. The extent of Msi-1 + IM cells was estimated semiquantitatively according to the percentage of stained cells among the total number of IM cells in each biopsy tissue section. The percentage of positive cells was divided into four grades; 0 (absent), 1 (< 20% of cells positive), 2 (20–50% of cells positive), and 3 (> 50% of the cells positive).

### DOUBLE-LABELLING

The combinations used in the immunohistochemical double-labelling were rat anti-mouse Msi-1 antibody plus either mouse anti-human PCNA (dilution 1 : 100; Dako), Ki67 (1 : 50; Dako), MUC5AC (1 : 100; Zymed Laboratories, South San Francisco, CA, USA), MUC6 (NCL-MUC-6, 1 : 50; Novocastra, Newcastle, UK) or TFF1 (pS2, 1 : 100; Zymed) antibody as the primary antibodies, and biotinylated goat anti-rat antibody (Dako) plus alkaline phosphatase-conjugated goat anti-mouse antibody (Dako) as the secondary antibodies.<sup>19</sup> The sections were treated with alkaline phosphatase substrate solution (New fuchsin substrate system; Dako) to develop the alkaline phosphatase and allow visualization of the antigens.

The combination used in immunofluorescent double-labelling was rat anti-mouse Msi-1 antibody plus mouse anti-human PCNA antibody (1 : 100; Dako) as the primary antibodies, and Texas red-conjugated rabbit anti-rat antibody (Vector Laboratories, Ontario, Canada) plus fluorescein-conjugated horse anti-mouse antibody (Vector) as the secondary antibodies.<sup>20</sup> The

images were captured by confocal microscopy using a BioRad RADIANCE 2100 laser scanning system (BioRad, Hercules, CA, USA).

#### WESTERN BLOT ANALYSIS

Frozen stomach tissue samples were obtained from one of the 33 surgically resected stomachs described above. For detection of the Msi-1 protein by immunoblotting, the tissue samples were homogenized in radio-immunoprecipitation assay lysis buffer [1% Nonidet P-40, 0.1% sodium dodecyl sulphate (SDS), 100 µg/ml phenylmethyl sulfonyl fluoride (PMSF), 0.5% sodium deoxycholate, 1 mM sodium orthovanadate, 2 µg/ml aprotinin, 2 µg/ml antipain, and 2 µg/ml leupeptin in PBS] on ice, and after centrifugation at 13 000 *g* at 4°C for 20 min, the supernatants were collected.<sup>21</sup> Protein concentration was determined by using the Bradford assay (BioRad), and tissue lysates were mixed with an equal amount of 2 × SDS loading buffer (100 mM Tris-HCl, 4% SDS, 20% glycerol, and 0.2% bromophenol blue), as described previously.<sup>22</sup> Samples were heated at 100°C for 5–10 min before loading and separated on 12% SDS-polyacrylamide gels (BioRad). The proteins were electrotransferred to a nitrocellulose membrane (Amersham, Arlington Heights, IL, USA) in transfer buffer containing 48 mM Tris-HCl, 39 mM glycine, 0.037% SDS, and 20% methanol at 4°C for 1 h. Non-specific binding to the membrane was blocked for 1 h at room temperature with 5% Carnation non-fat milk in Tris-buffered saline (TBS) buffer (20 mM Tris-HCl, 150 mM NaCl, and 0.1% Tween 20). The membranes were then incubated for 16 h at 4°C with the Msi-1 antibody in blocking buffer containing 5% non-fat milk. The Msi-1 antibody was diluted to a final concentration of 1 µg/ml. Following extensive washing in TBS buffer, the membranes were incubated with a goat anti-rat IgG antibody conjugated with alkaline phosphatase (Promega, Madison, WI, USA) for 1 h at room temperature

in 5% non-fat milk dissolved in TBS. Membranes were then washed with TBS buffer, and immunoreactive bands were visualized by incubation of the membrane with 5-bromo-4-chloro-3-indolyl-phosphate (BIPC)/nitroblue tetrazolium (NBT) colour substrate according to the manufacturer's protocol (Promega).

## Results

#### Msi-1 EXPRESSION IN THE PROLIFERATIVE REGIONS OF THE ADULT HUMAN ANTRUM

In the adult human antrum, Msi-1 expression was observed predominantly in the epithelial cells of the isthmus/neck region. The cytoplasm of these epithelial cells was strongly positive for Msi-1 (Figure 1A). Many of the Msi-1+ cells were round, morphologically immature cells with a small amount of cytoplasm and a dark nucleus (Figure 1B). In contrast, the surface epithelial cells in the upper part of the pit and the epithelial cells in the basal regions of the glands were completely negative for Msi-1 expression (Figure 1A). In addition, specific expression of Msi-1 was not found in any regions of the fundic glands.

To examine the relationship between the Msi-1+ cells and the proliferative cells in the gastric glands of the human antrum, we double-stained for Msi-1 and PCNA. The proliferative regions were characterized by PCNA+ epithelial cells and were located in the isthmus/neck region. Msi-1+ cells were located mainly in the lower parts of the proliferative regions (Figure 1C). Although the Msi-1+ cells were intermingled with the PCNA+ cells in the proliferative regions, the Msi-1+ cells showed no PCNA expression, and no double-positive cells were found in any regions (Figure 1D). A further confirmatory study of immunofluorescent double-labelling for PCNA and Msi-1 using confocal laser scanning microscopy clearly demonstrated that Msi-1+ cells were not colocalized with PCNA+

**Figure 1.** Msi-1 expression in the proliferative regions of the adult human antrum. **A**, In the antral mucosa, the pits usually occupy approximately half of the mucosal thickness. Msi-1+ cells (arrow) are present in the epithelial cells of the isthmus/neck region. **B**, Higher magnification of the rectangular portion marked in **A**. Msi-1+ cells can be seen in the isthmus/neck region as round cells with small amounts of cytoplasm and dark nuclei. The arrow points to a morphologically immature cell expressing Msi-1. **C**, Double-staining for proliferating cell nuclear antigen (PCNA) and Msi-1 in the gastric glands of the antral mucosa. The arrows indicate PCNA+ nuclei (red labelling), which are distributed throughout the epithelial cells in the isthmus/neck region. The arrowheads indicate Msi-1+ cells (brown labelling), which are intermingled with the PCNA+ cells, are present in the lower part of the isthmus/neck region. **D**, Higher magnification of Msi-1+ cells within the proliferative region. Msi-1 reactivity (brown labelling) is present in the cytoplasm, while PCNA reactivity (red labelling) is restricted to the nucleus. The arrowheads indicate cells with an Msi-1+ cytoplasm but devoid of nuclear PCNA staining. The double-staining was visualized using DAB (brown labelling) and fuchsin (red labelling) substrates. **E**, Double-staining for PCNA and Msi-1 using confocal laser scanning microscopy. The arrows indicate cells with Msi-1+ cytoplasm (red labelling) but no nuclear PCNA staining (green labelling). The arrowheads indicate PCNA+ nuclei. **F**, Double-staining for Msi-1 and Ki67 in the gastric glands of the antral mucosa. The arrows indicate cells with Msi-1+ cytoplasm (brown labelling) but devoid of nuclear Ki67 staining (red labelling). The arrowheads indicate Ki67+ nuclei. The double-staining was visualized using DAB (brown labelling) and fuchsin (red labelling) substrates. Bars are 50 µm (**A**), 40 µm (**B**), 40 µm (**C**), 30 µm (**D**), 7 µm (**E**), and 30 µm (**F**).

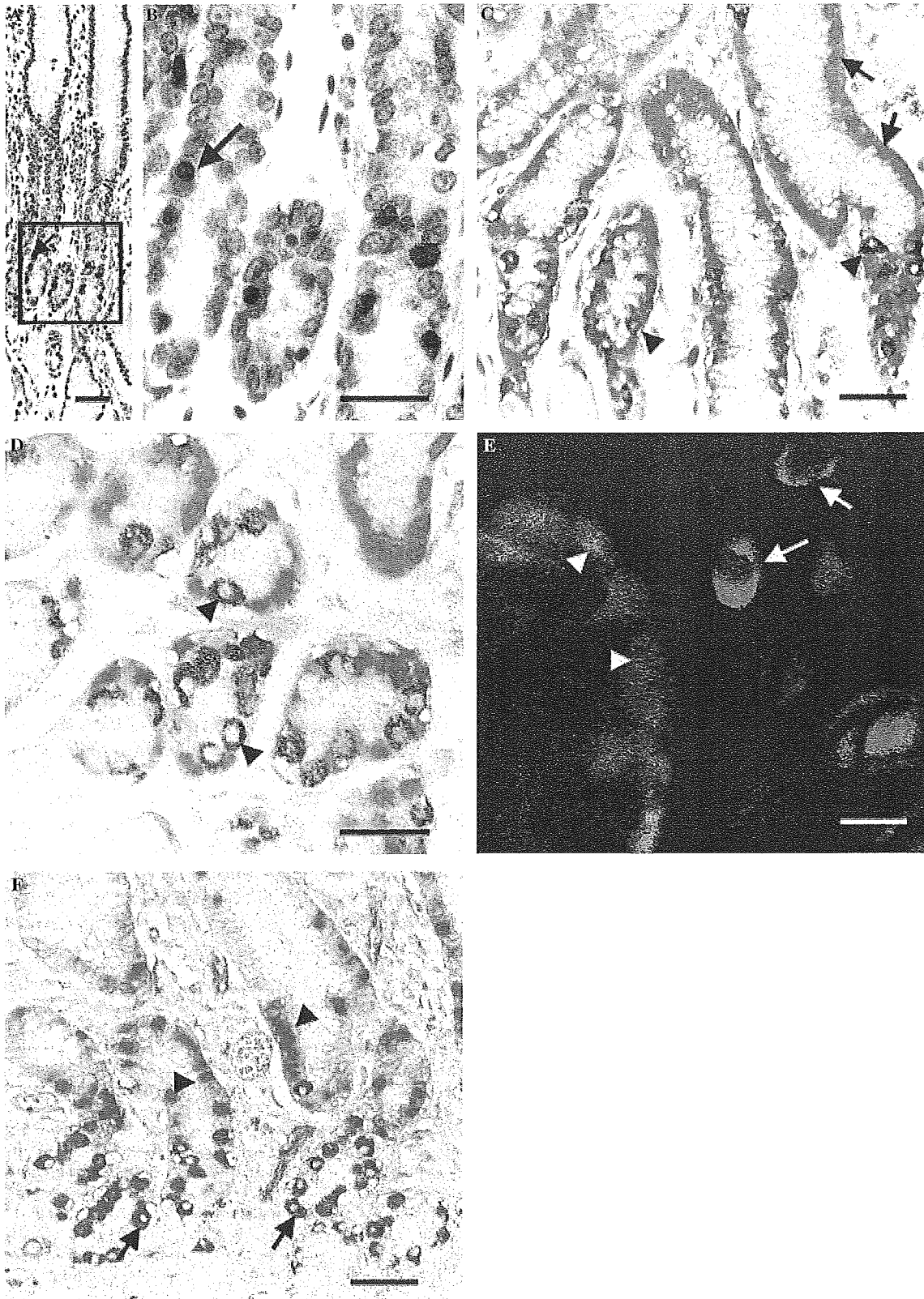




Figure 2. Western blot demonstrating the expression of Msi-1 protein in the human antrum. Frozen tissue samples from the antral, body and fundic mucosa were obtained from the same surgically resected human stomach. Whole tissue lysates (60 µg) were loaded on 12% SDS-PAGE gels. Pairs of positive bands (the pair being due to the presence of splice variants) are observed in the antral (lane 1) and body mucosa (lane 2) at the same molecular weight (37 kDa) as observed in embryonic mouse brain.<sup>14,16</sup> The tissue sample from the fundic mucosa (lane 3) yields a faint band, but no pair. A pair of positive bands in the body mucosa may be due to the detection of pyloric glands extended from the antral area to the body area.

cells (Figure 1E). A similar pattern was obtained on double-staining for Msi-1 and Ki67, although there were fewer Ki67+ cells than PCNA+ cells (Figure 1F).

#### WESTERN BLOT ANALYSIS

The presence of Msi-1 expression in the adult human stomach was confirmed by Western blot analysis. On Western blot analysis using the Msi-1 antibody, a pair of positive bands (37 kDa) was observed in embryonic mouse brain, due to the presence of splice variants.<sup>14,16</sup> Similarly, in the present study, a pair of positive bands was observed in the antral mucosa of the human stomach at the same molecular weight as in embryonic mouse brain (Figure 2),<sup>14,16</sup> confirming the presence of Msi-1 protein in the human antrum. In contrast, the tissue sample from the fundic mucosa yielded a faint band, but not a pair, indicating absence of Msi-1 protein in the fundic mucosa.

#### Msi-1 EXPRESSION DURING DEVELOPMENT OF THE HUMAN STOMACH

By the 14th to the 17th weeks of gestation, gastric pits, neck regions, early glands and surface epithelial cells are present in most parts of the stomach. In the present study, Msi-1 expression during the 14th week was found to be concentrated in the epithelial cells in the basal regions of the pyloric glands (Figure 3A). By the 19th week, Msi-1+ cytoplasm was seen predominantly in the epithelial cells in the basal regions of the pyloric glands, although cells with PCNA+ nuclei were scattered throughout the entire epithelial cell population (Figure 3B). By the 20th to the 27th weeks, the number of Msi-1+ cells had increased; these cells were located predominantly in the lower to middle portions of the gastric glands of the antrum (Figure 3C). By the

22nd week, the PCNA+ cells had mostly moved to a higher position than the Msi-1+ cells, and the PCNA+ cells were concentrated in the epithelial cells in the pit regions of the glands (Figure 3C). The Msi-1+ cells showed no PCNA expression, as similarly seen in the gastric glands of adult human antrum (see the first section of Results).

#### PARTIAL COLOCALIZATION OF Msi-1 AND GASTRIC-TYPE MUCINS IN THE ADULT HUMAN ANTRUM

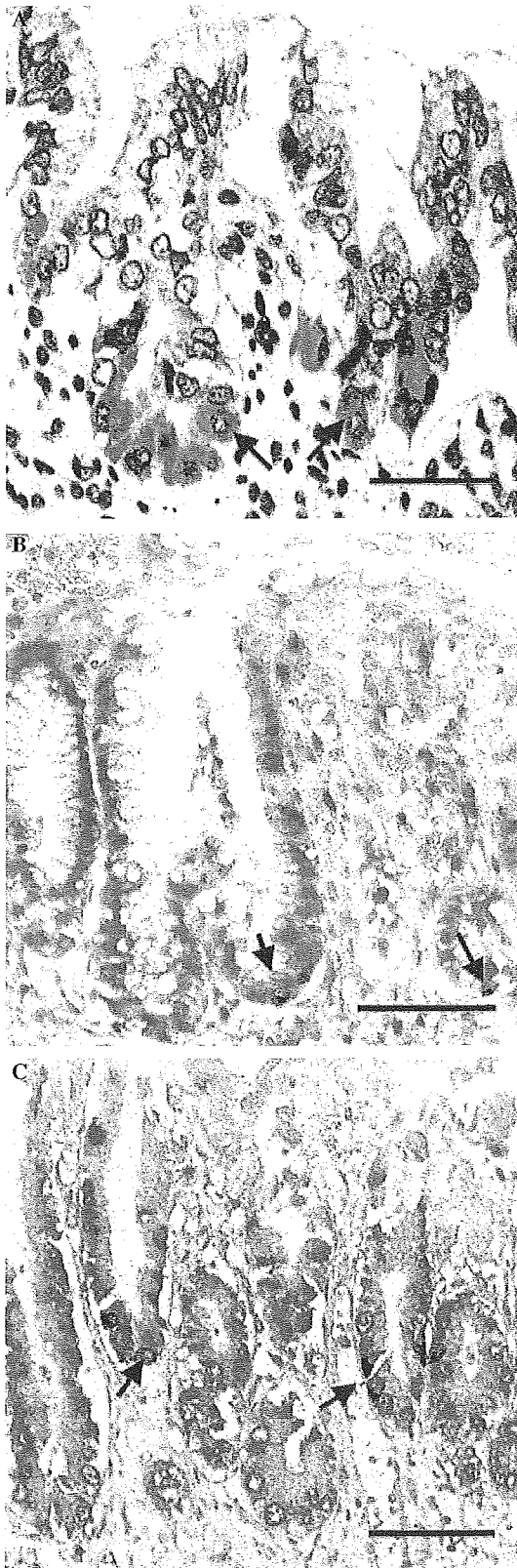
MUC5AC was strongly expressed by the surface epithelial and neck cells of both the gastric body and the antrum. On the other hand, MUC6 was expressed mainly in the pyloric gland cells of the antrum, following similar patterns to those described previously.<sup>23</sup> Double-staining for MUC6 and Msi-1 revealed that the distributions of the two antigens overlapped partly, and that Msi-1 expression was generally limited to the upper regions of MUC6+ glands (Figure 4A). Double-staining for MUC5AC and Msi-1 again demonstrated that the distributions of the two antigens overlapped partly and that Msi-1 expression was generally limited to the lower regions of the MUC5AC+ glands (Figure 4B). TFF1 expression, which is generally observed in the foveolar pit area, was less extensive than MUC5AC expression and coexpression of TFF1 and Msi-1 was not usually detected (Figure 4C).

#### DECREASED EXPRESSION OF Msi-1 IN IM

In the gastric glands showing IM, Msi-1 expression became weaker than in the gastric glands without IM (Figure 5A). Msi-1 expression was detectable predominantly in the cytoplasm of goblet and columnar cells, but was occasionally found in the nucleus. In the gastric glands showing incomplete IM, Msi-1 expression was detected in 15 out of the 31 specimens (48.4%); however, > 50% positivity was found in only one specimen (Table 1). In the gastric glands showing complete IM (Figure 5B), no Msi-1 reactivity was detected in 24 out of the 31 tissue samples (77.4%), and > 50% positivity was not found in any specimen (Table 1). The percentages of Msi-1 positivity in complete IM were lower than those in incomplete IM at all levels of Msi-1 reactivity (Table 1).

#### Discussion

As in the fetal rat stomach,<sup>24,25</sup> during the earliest stages of development of the human stomach, the proliferative regions (progenitor zones) are located in the basal regions of the glands. As development of the pit

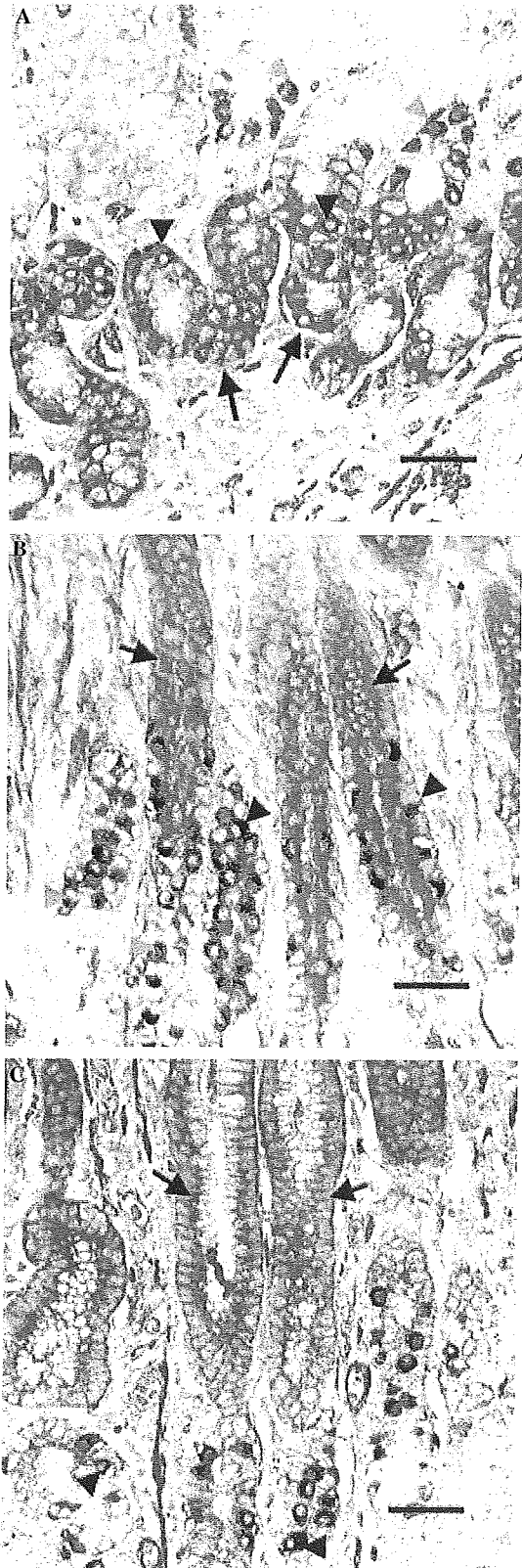


gland proceeds, the proliferative region moves upwards, and is limited to the isthmus/neck region in the adult human stomach.<sup>24</sup> The changing pattern of distribution of the proliferative regions is similar to that of the localization of Msi-1+ cells in the developing gastric glands. Msi-1 expression was present specifically in the basal regions of early glands and subsequently moved upwards, finally establishing an adult location in the isthmus/neck region, where adult putative progenitor cells are thought to be actively proliferating. Indeed, in the present study, double-staining for Msi-1 and PCNA demonstrated that Msi-1+ cells were located among the actively proliferating cells in the isthmus/neck region of the adult human antrum. These results indicate that the transient expression of Msi-1 coincides well with the actively proliferative regions containing progenitor cells in both fetal and adult gastric glands in the antrum. A similar trend in the expression pattern of Msi-1 has been reported in the mouse small intestine, where Msi-1 is expressed specifically within the small intestinal crypts, and putative stem cells and at least the next two generations are positive for Msi-1.<sup>15</sup> The positive correlation between the distribution of Msi-1+ cells and that of the proliferative regions in the gastric glands suggests that Msi-1+ cells have progenitor cell characteristics in the human antrum.<sup>6</sup>

A previous study has shown that Msi-1 expression correlates well with the proliferative activity of human brain tumours.<sup>26</sup> Similarly, Msi-1+ neural stem and progenitor cells induced by ischaemia in the rat hippocampus show bromodeoxyuridine expression.<sup>20</sup> These observations indicate that Msi-1 expression can correlate positively with proliferative activity in these

**Figure 3.** Msi-1 expression in the fetal human antrum. **A**, By the 14th week of gestation, the pit/gland structure has elongated, while the surface columnar epithelial cells have differentiated and exhibit cytoplasm with basal nuclei. Msi-1 expression (arrows) is concentrated in the basal regions of the pyloric glands. **B**, Double-staining for proliferating cell nuclear antigen (PCNA) and Msi-1 in the pyloric glands at the 19th week of gestation. Cells with Msi-1+ cytoplasm (brown labelling) are seen predominantly in the epithelial cells in the basal regions of the pyloric glands, although cells with PCNA+ nuclei (red labelling) are scattered throughout the entire epithelial cell population. The arrows indicate cells with an Msi-1+ cytoplasm. **C**, Double-staining for PCNA and Msi-1 in the gastric glands of the antrum at the 22nd week of gestation. Along with a concomitant increase in the heights of the pits and glands, the PCNA+ cells are concentrated in the epithelial cells in the pit regions of the glands. By the 22nd week of gestation, most cells with PCNA+ nuclei (red labelling) have moved to a higher position than cells with Msi-1+ cytoplasm (brown labelling). The arrows indicate cells with an Msi-1+ cytoplasm but devoid of nuclear PCNA staining. The double-staining was visualized using DAB (brown labelling) and fuchsin (red labelling) substrates. Bars are 20  $\mu$ m (A), 40  $\mu$ m (B), and 40  $\mu$ m (C).





cell types.<sup>26–28</sup> Supportive evidence has been reported in the amphibian gastrointestinal tract during metamorphosis, in which Msi-1 and PCNA are coexpressed in the stomach.<sup>6</sup> However, in the present study the Msi-1+ cells in the proliferative regions showed no PCNA or Ki67 expression. A functional *in vitro* study of Msi-1 has shown that Notch signalling activity is increased by Msi-1 expression.<sup>29</sup> Activation of the Notch signalling pathway suppresses the differentiation of stem cells and plays a fundamental role in maintaining cells in an undifferentiated state. This suggests that the Msi-1+ cells within the proliferative regions of the human antrum may remain in an undifferentiated state and not express PCNA or Ki67.<sup>30</sup> Along with the partial differentiation of Msi-1+ cells, the Msi-1+ cells may begin to proliferate actively, which leads to the rapid down-regulation of Msi-1 expression together with the expression of PCNA or Ki67. Therefore, Msi-1 can be useful for identifying progenitor cells before active proliferation in the human antrum.

Specific antibodies against the various mucins are used to define gastric phenotypes. These include the MUC5AC antibody, which is specific for gastric foveolar-type mucin, and the MUC6 antibody, which is specific for pyloric gland-type mucin.<sup>31</sup> In the present study, the distribution of Msi-1 overlapped partly with that of MUC5AC and MUC6. Furthermore, Msi-1 expression was generally limited to the upper regions of the glands positive for MUC5AC and the lower regions of the glands positive for MUC6. Since epithelial cell differentiation and gastric gland migration are thought to be closely linked,<sup>24,25</sup> Msi-1+ cells located in the upper or lower glandular regions could move upwards or downwards, and then differentiate into foveolar or pyloric gland cells, respectively. This suggests that Msi-1+ cells retain at least some features

**Figure 4.** Partial colocalization of Msi-1 and gastric-type mucins in the adult human antrum. **A,** The arrows indicate MUC6+ cells (red labelling), which are almost all present among the epithelial cells in the pyloric glands. The black arrowheads indicate Msi-1+ cells (brown labelling), which are located mainly in the upper region of the MUC6+ glands. MUC6 expression gradually decreases toward the upper region of the glands, and Msi-1+ cells devoid of MUC6 expression (blue arrowheads) are visible. **B,** The arrows indicate MUC5AC+ cells (red labelling), which are almost all present throughout the foveolar cell population. The black arrowheads indicate Msi-1+ cells (brown labelling), which are located mainly in the lower regions of the MUC5AC+ glands. Msi-1+ cells devoid of MUC5AC expression (blue arrowheads) are also detected. **C,** There is no coexpression of TFF1 and Msi-1 in the gastric glands of the antrum. The arrows indicate TFF1+ cells (red labelling) and the arrowheads indicate Msi-1+ cells (brown labelling). The double-staining was visualized using DAB (brown labelling) and fuchsin (red labelling) substrates. All bars are 50  $\mu$ m.

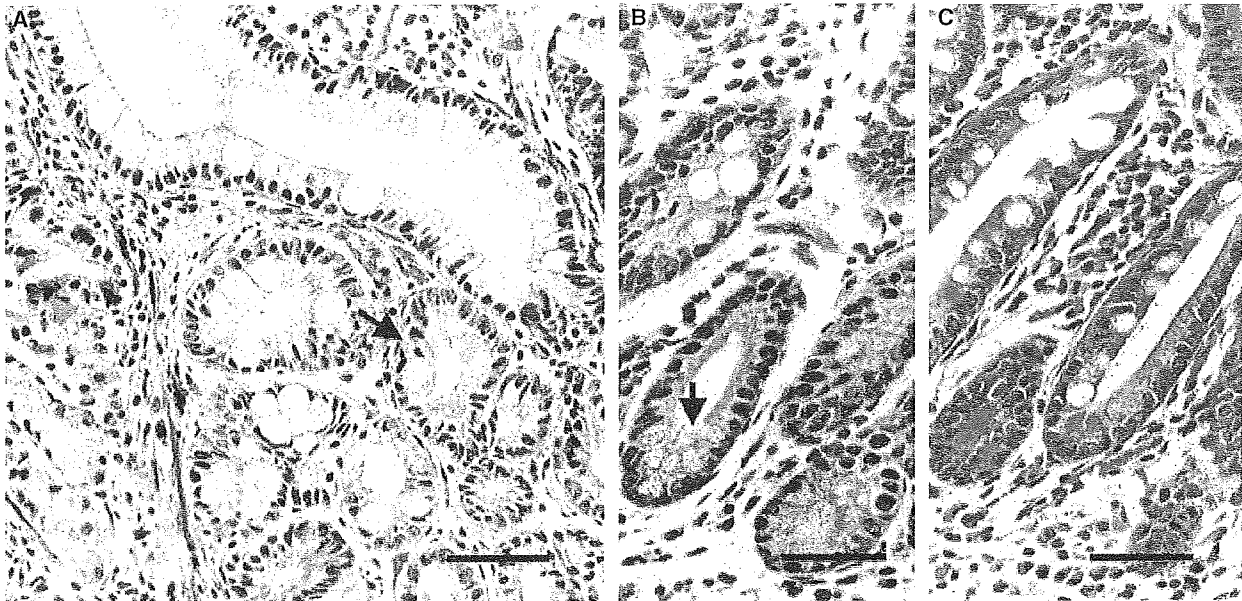


Figure 5. Decreased expression of Msi-1 in intestinal metaplasia (IM). A, Msi-1 expression in incomplete IM becomes weaker than that in the gastric glands without IM. The arrow indicates the Msi-1+ metaplastic epithelial cell and the blue arrowhead indicates the Msi-1+ epithelial cell in the gastric glands without IM. B, Weak Msi-1 expression is detected in the metaplastic epithelial cells of complete IM. The arrow indicates Msi-1 reactivity in the cytoplasm of the epithelial cell adjacent to Paneth cells. C, H&E-stained serial section from the metaplastic region of complete IM in B. All bars are 50 µm.

**Table 1.** Grading of reactive cells in each Msi-1 staining of intestinal metaplasia (IM) glands in human stomach

Type of IM	Grading by percentage of reactive cells				Total number of tissue samples
	Grade 0	Grade 1	Grade 2	Grade 3	
Incomplete	0	0 < x < 20%	20% < x < 50%	50% < x	31
Complete	16 (51.6%)	8 (25.8%)	6 (19.3%)	1 (3.2%)	31
	24 (77.4%)	6 (19.3%)	1 (3.2%)	0	31

characteristic of both foveolar and pyloric gland cell differentiation phenotypes.

Another interesting finding of the present study is that Msi-1 expression is decreased in the IM cells of the human stomach. Several recent studies have indicated that Msi-1 appears to be preferentially expressed in the early generations of cell lineages in mouse small intestine and colon.<sup>15,32</sup> In the present study, however, Msi-1 expression was markedly decreased in IM cells of the human stomach. The difference in the patterns of Msi-1 expression between normal intestine and metaplasia supports the assumption that IM is a consequence of abnormal differentiation, in which, as has previously been proposed,<sup>33</sup> stem cells or progenitor cells may not differentiate into any of the normal intestinal epithelial phenotypes. At the present time, the mechanism governing Msi-1 protein expression in the adult human antrum is still unknown. Functional

studies are needed to clarify the characteristics of Msi-1+ cells as progenitor cells and the role of Msi-1 protein in the regulation of normal epithelial cell differentiation and metaplastic change in the human antrum.

## References

1. Kirkland SC. Clonal origin of columnar, mucous, and endocrine cell lineages in human colorectal epithelium. *Cancer* 1988; 61: 1359–1363.
2. Ponder BA, Schmidt GH, Wilkinson MM *et al*. Derivation of mouse intestinal crypts from single progenitor cells. *Nature* 1985; 313: 689–691.
3. Brittan M, Wright NA. Gastrointestinal stem cells. *J. Pathol.* 2002; 197: 492–509.
4. Modlin IM, Kidd M, Lye KD, Wright NA. Gastric stem cells: an update. *Keio J. Med.* 2003; 52: 134–137.
5. Brittan M, Wright NA. Stem cell in gastrointestinal structure and neoplastic development. *Gut* 2004; 53: 899–910.



6. Ishizuya-Oka A, Shimizu K, Sakakibara S, Okano H, Ueda S. Thyroid hormone-upregulated expression of Musashi-1 is specific for progenitor cells of the adult epithelium during amphibian gastrointestinal remodeling. *J. Cell Sci.* 2003; **116**: 3157–3164.
7. Hattori T, Fujita S. Tritiated thymidine autoradiographic study of cell migration and renewal in the pyloric mucosa of golden hamsters. *Cell Tissue Res.* 1976; **175**: 49–57.
8. Karam SM, Leblond CP. Dynamics of epithelial cells in the corpus of the mouse stomach. I. Identification of proliferative cell types and pinpointing of the stem cell. *Anat. Rec.* 1993; **236**: 259–279.
9. Karam SM, Leblond CP. Dynamics of epithelial cells in the corpus of the mouse stomach. II. Outward migration of pit cells. *Anat. Rec.* 1993; **236**: 280–296.
10. Karam SM, Straiton T, Hassan WM, Leblond CP. Defining epithelial cell progenitors in the human oxyntic mucosa. *Stem Cells* 2003; **21**: 322–336.
11. Nakamura M, Okano H, Blendy JA, Montell C. Musashi, a neural RNA-binding protein required for *Drosophila* adult external sensory organ development. *Neuron* 1994; **13**: 67–81.
12. Sakakibara S, Imai T, Hamaguchi K *et al.* Mouse-Musashi-1, a neural RNA-binding protein highly enriched in the mammalian CNS stem cell. *Dev. Biol.* 1996; **176**: 230–242.
13. Good P, Yoda A, Sakakibara S *et al.* The human Musashi homolog 1 (MSH1) gene encoding the homologue of Musashi/Nrp-1, a neural RNA-binding protein putatively expressed in CNS stem cells and neural progenitor cells. *Genomics* 1998; **52**: 382–384.
14. Kaneko Y, Sakakibara S, Imai T *et al.* Musashi1: an evolutionally conserved marker for CNS progenitor cells including neural stem cells. *Dev. Neurosci.* 2000; **22**: 139–153.
15. Kayahara T, Sawada M, Takaishi S *et al.* Candidate markers for stem and early progenitor cells, Musashi-1 and Hes1, are expressed in crypt base columnar cells of mouse small intestine. *FEBS Lett.* 2003; **535**: 131–135.
16. Potten CS, Booth C, Tudor GL *et al.* Identification of a putative intestinal stem cell and early lineage marker: musashi-1. *Differentiation* 2003; **71**: 28–41.
17. Kawachi T, Kogure K, Tanaka N, Tokunaga A, Sugimura T. Studies of intestinal metaplasia in the gastric mucosa by detection of disaccharidases with 'Tes-Tape'. *J. Natl Cancer Inst.* 1974; **53**: 19–30.
18. Kanemura Y, Sakakibara S, Okano H. Identification of Musashi1-positive cells in human normal and neoplastic neuroepithelial tissues by immunohistochemical methods. *Meth. Mol. Biol.* 2002; **198**: 273–281.
19. Waiser J, Schwaar S, Bohler T *et al.* Immunohistochemical double-staining of renal allograft tissue: critical assessment of three different protocols. *Virchows Arch.* 2002; **440**: 648–654.
20. Yagita Y, Kitagawa K, Ohtsuki T *et al.* Neurogenesis by progenitor cells in the ischemic adult rat hippocampus. *Stroke* 2001; **32**: 1890–1896.
21. Liu Y, Tolbert EM, Lin L *et al.* Up-regulation of hepatocyte growth factor receptor: an amplification and targeting mechanism for hepatocyte growth factor action in acute renal failure. *Kidney Int.* 1999; **55**: 442–453.
22. Yang J, Dai C, Liu Y. Hepatocyte growth factor gene therapy and angiotensin II blockade synergistically attenuate renal interstitial fibrosis in mice. *J. Am. Soc. Nephrol.* 2002; **13**: 2464–2477.
23. Reis CA, David L, Correa P *et al.* Intestinal metaplasia of human stomach displays distinct patterns of mucin (MUC1, MUC2, MUC5AC, and MUC6) expression. *Cancer Res.* 1999; **59**: 1003–1007.
24. Menard D, Arsenaault P. Cell proliferation in developing human stomach. *Anat. Embryol.* 1990; **182**: 509–516.
25. Yang DH, Tsuyama S, Ge YB *et al.* Proliferation and migration kinetics of stem cells in the rat fundic gland. *Histol. Histopathol.* 1997; **12**: 719–727.
26. Okano H, Imai T, Okabe M. Musashi: a translational regulator of cell fate. *J. Cell Sci.* 2002; **115**: 1355–1359.
27. Kanemura Y, Mori K, Sakakibara S *et al.* Musashi1, an evolutionarily conserved neural RNA-binding protein, is a versatile marker of human glioma cells in determining their cellular origin, malignancy, and proliferative activity. *Differentiation* 2001; **68**: 141–152.
28. Toda M, Iizuka Y, Yu W *et al.* Expression of the neural RNA-binding protein Musashi1 in human gliomas. *Glia* 2001; **34**: 1–7.
29. Imai T, Tokunaga A, Yoshida T *et al.* The neural RNA-binding protein Musashi1 translationally regulates mammalian numb gene expression by interacting with its mRNA. *Mol. Cell Biol.* 2001; **21**: 3888–3900.
30. Sakakibara S, Nakamura Y, Yoshida T *et al.* RNA-binding protein Musashi family: roles for CNS stem cells and a subpopulation of ependymal cells revealed by targeted disruption and antisense ablation. *Proc. Natl Acad. Sci. USA* 2002; **99**: 15194–15199.
31. Shiroshita H, Watanabe H, Ajioka Y *et al.* Re-evaluation of mucin phenotypes of gastric minute well-differentiated-type adenocarcinomas using a series of HGM, MUC5AC, MUC6, M-GGMC, MUC2 and CD10 stains. *Pathol. Int.* 2004; **54**: 311–321.
32. Nishimura S, Wakabayashi N, Toyoda K, Kashima K, Mitsufuji S. Expression of Musashi-1 in human normal colon crypt cells: a possible stem cell marker of human colon epithelium. *Dig. Dis. Sci.* 2003; **48**: 1523–1529.
33. Tatematsu M, Tsukamoto T, Inada K. Stem cells and gastric cancer: role of gastric and intestinal mixed intestinal metaplasia. *Cancer Sci.* 2003; **94**: 135–141.

# The RNA-binding protein HuD regulates neuronal cell identity and maturation

Wado Akamatsu<sup>\*†</sup>, Hiroaki Fujihara<sup>‡</sup>, Takayuki Mitsuhashi<sup>§</sup>, Masato Yano<sup>\*</sup>, Shinsuke Shibata<sup>\*</sup>, Yoshika Hayakawa<sup>\*¶</sup>, Hiroataka James Okano<sup>\*</sup>, Shin-ichi Sakakibara<sup>||</sup>, Hiroshi Takano<sup>\*\*</sup>, Toshiya Takano<sup>‡</sup>, Takao Takahashi<sup>§</sup>, Tetsuo Noda<sup>\*\*</sup>, and Hideyuki Okano<sup>\*††††</sup>

Departments of <sup>\*</sup>Physiology, <sup>‡</sup>Microbiology, and <sup>§</sup>Pediatrics, Keio University School of Medicine, Tokyo 160-8582, Japan; <sup>||</sup>Department of Histology and Neurobiology, Dokkyo University School of Medicine, Tochigi 321-0293, Japan; <sup>\*\*</sup>Department of Molecular Genetics, Tohoku University School of Medicine, Sendai 980-8575, Japan; and <sup>††</sup>Core Research for Evolutional Science and Technology, Japan Science and Technology Agency, Saitama 332-0012, Japan

Edited by Yuh Nung Jan, University of California School of Medicine, San Francisco, CA, and approved February 4, 2005 (received for review October 11, 2004)

Neural Hu proteins (HuB/C/D) are RNA-binding proteins that have been shown to induce neuronal differentiation activity when overexpressed in immature neural progenitor cells or undifferentiated neuronal tumors. Newly generated *HuD*-deficient mice exhibited a transient impaired-cranial-nerve-development phenotype at an early embryonic stage. Adult *HuD*-deficient mice exhibited an abnormal hind-limb reflex and poor rotarod performance. Analysis of neurosphere formation revealed that the number and self-renewal capacity of the neural stem/progenitor cells were increased in *HuD*-deficient mice. *HuD*-deficient primary neurospheres also generated a smaller number of neurons. Cohort analysis of the cellular proliferative activity by using BrdUrd and iododeoxuridine labeling revealed that the number of differentiating quiescent cells in the embryonic cerebral wall was decreased. Long-term administration of BrdUrd revealed that the number of slowly dividing stem cells in the adult subventricular zone was increased in the *HuD*-deficient mice. Taken together, the results suggest that HuD is required at multiple points during neuronal development, including negative regulation of proliferative activity and neuronal cell-fate acquisition of neural stem/progenitor cells.

ELAV | Hu | neural stem cell

Hu proteins have been identified as the target antigens of autoantibodies appearing in the sera of patients with paraneoplastic encephalomyelitis (1). By molecular cloning, four members of the Hu protein family have been identified as RNA-binding proteins that resemble the *Drosophila* ELAV protein (1–4). These mammalian Hu/ELAV proteins, with the exception of HuA (HuR), are widely expressed in both early postmitotic and mature neurons; HuA (HuR), however, is expressed ubiquitously. All members of the Hu family proteins contain three RNA-recognition motifs, and their structures are highly conserved. Previous reports have suggested the binding of Hu proteins to several putative target mRNAs, both *in vitro* and *in vivo*. Because most of the target mRNAs have AU-rich elements in their untranslated regions, Hu proteins possibly regulate the stability or translational efficiency of their target mRNAs. Most of these putative target genes are involved in cellular proliferation [p21 (5), p27 (6), c-fos, and N-Myc (7)] or are important in the formation of neurites [Neurofilament-M (8), GAP-43 (9), and tau (10, 11)].

Thus, Hu proteins have been considered to be involved in the differentiation and/or maintenance of neurons. Previously, we reported, by a gene transfer experiment conducted with the electroporation method, that overexpression of HuB/HuC induces neuronal differentiation in PC12 cells and in the periventricular immature neural stem or progenitor cells of embryonic mice (12). *HuD* has also been shown to have similar functions in PC12 cells (13). It has been also reported that antisense-mediated knockdown of HuC results in impaired spatial learning performance in mice, with concomitant down-regulation of GAP-43 expression (14).

These findings indicate the possible involvement of the Hu proteins in the sprouting and regeneration of neurons. In this paper, we report on the phenotype of mice with targeted disruption of the *HuD* gene, whose expression commences even earlier than that of HuC, another member of the same family (4), and continues to be seen even in mature neurons.

## Materials and Methods

**Generation of *HuD*-Deficient mice.** *HuD*-deficient mice were generated by a method similar to one described previously (15). Briefly, a 2.5-kb fragment containing intronic sequences upstream and a 6.1-kb fragment containing intronic sequences downstream of the second exon that contains the second RNA-recognition motifs (25–265 bp of cDNA) were inserted into the target plasmid vector to delete a 1.0-kb genomic DNA fragment and induce a frame shift. RT-PCR analysis was performed by using the primers 5'-AGAAGGGAATGTGTCAGCTTTT-3' (exon 1) and 5'-TGAATTCCTCTGGGTCATA-3' (exon 2), or 5'-TATGACCCAAGAGGAATTCA-3' (exon 2) and 5'-TGGTCTTGGGAAGGCCACTA-3' (exon 3).

Immunoblotting was performed with the same method as described (12). Anti-HuD monoclonal antibody 16C12 (Clonogene, Hartford, CT) was used in 1:500 dilutions. Anti-HuB/C/D human serum (a gift from Robert Darnell, The Rockefeller University, New York) was used in 1:2,000 dilutions.

**Whole-Mount Immunohistochemistry.** Whole-mount immunohistochemistry of the embryonic mice was performed as described (16).

**Analysis of Motor Functions.** Mice of each genotype that were 20–26 weeks old were used for the analysis. Each mouse was placed on a 3.5-cm-diameter rod covered with rubber to evaluate its rotarod performance: The mice were left on the rod for 1 min for habituation. The rotarod was then rotated at 20 rpm, and the performance of the mice was measured in terms of latency (time successfully spent on the rotating rod without falling off). Six trials were conducted for each individual. Mice that stayed on the rotarod for 300 s were considered complete responders, and their latencies were recorded as 300 s.

**Cell Culture and Immunocytochemistry.** Cells from the ganglionic eminence or cerebral cortex of embryonic day (E)14.5 embryos

This paper was submitted directly (Track II) to the PNAS office.

Abbreviations: IdUrd, iododeoxuridine; SVZ, subventricular zone; En, embryonic day *n*; P, proliferative; Q, quiescent.

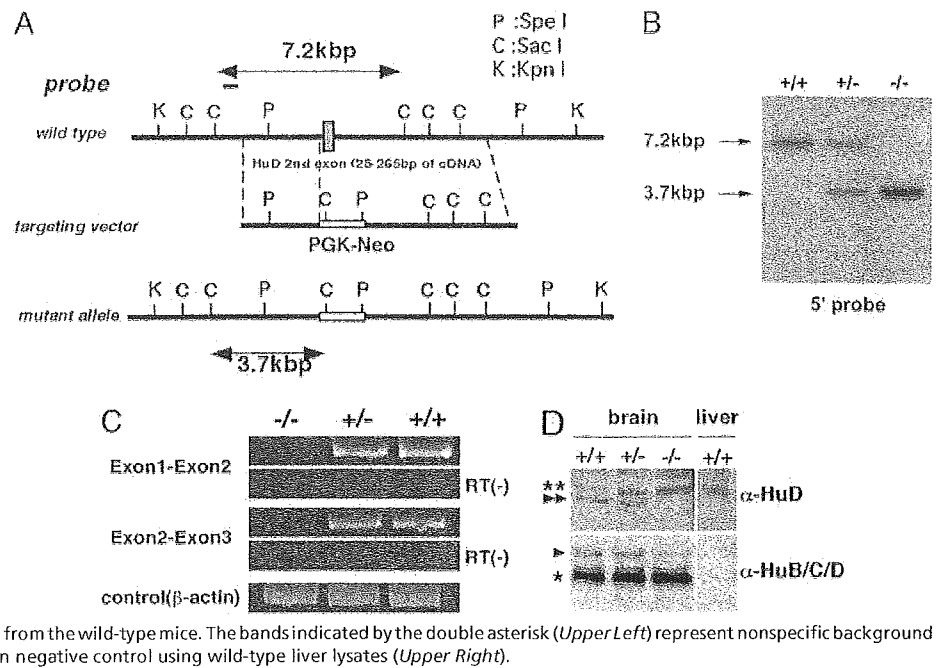
<sup>†</sup>To whom correspondence may be sent at the present address: Department of Medical Genetics and Microbiology, University of Toronto, 1 King's College Circle, Toronto, ON, Canada M5S 1A8. E-mail: wado.akamatsu@utoronto.ca.

<sup>¶</sup>Present address: Department of Neurobiology, Graduate School of Medicine, Gifu University, Gifu 501-1194, Japan.

<sup>††</sup>To whom correspondence should be addressed. E-mail: hidokano@sc.itc.keio.ac.jp.

© 2005 by The National Academy of Sciences of the USA

**Fig. 1.** Targeting strategy, germ-line transmission, and expression analysis of the *HuD* gene. (A) Organization of the target vector, the mouse *HuD* gene, and the allele resulting from homologous recombination. An exon (black box) of the *HuD* allele containing the initiation codon was replaced with a PGK-neocassette. A 0.7-kb *Bam*HI-*Eco*RI fragment (5' probe) was used to screen for recombinant alleles, and the sizes of the recombinant and wild-type fragments after *Sac*I digestion are shown (bidirectional arrows). (B) Germ-line transmission was confirmed by Southern blot analysis of *Sac*I-digested tail DNA from a litter of F<sub>1</sub> mice, using a 5' probe. (C) The deletion of the *HuD* mRNA from the adult brains of homozygous animals was confirmed by RT-PCR analysis. No amplified bands were observed from the RT samples of the *HuD*  $-/-$  brains, using either of the primer pairs (Exon 1-Exon 2 and Exon 2-Exon 3). (D) Immunoblots of adult brain or liver lysates with anti-HuD 16C12 monoclonal antibody (Upper) or anti-HuB/C/D serum (Lower). The bands indicated by a double arrowhead represent the HuD protein (Upper) and are missing in the liver lysates from the wild-type mice. The bands indicated by the double asterisk (Upper Left) represent nonspecific background immunoreactivity, which was also observed in negative control using wild-type liver lysates (Upper Right).



were cultured as described (17). For the differentiation assays of the neurospheres, neurospheres were plated as described (15). Subsequently, triple-label immunostaining was performed to examine their differentiation into neurons, astroglia, and oligodendroglia, as described (18).

**Cohort Analysis of Cellular Proliferation in the Embryonic Cerebral Wall.** This experimental concept was identical to one described previously (19), except that iododeoxyuridine (IdUrd) was used in place of tritiated thymidine. (Also see Fig. 6, which is published as supporting information on the PNAS web site.) Proliferating cells of the embryonic cerebral wall were exposed sequentially, by i.p. injection, to the S phase marker IdUrd (50 mg/g of body weight; Sigma) and BrdUrd (50 mg/g of body weight; Sigma). Briefly, IdUrd was injected at 8:00 a.m. in both (P + Q and Q) protocols. Then BrdUrd was injected at 10:00 a.m., 1:00 p.m., 4:00 p.m., and 7:00 p.m. in the protocol for Q. In the protocol for P + Q, BrdUrd was injected only at 10:00 a.m. Animals in both protocols were killed and fixed at 10:30 p.m. (14.5 h from initial IdUrd injection). These protocols yielded separate values for the number of Q cells [N(Q)] and P + Q cells [N(P + Q)] in 2 h (8:00–10:00 a.m.) cohort (19) (for details, see Fig. 6 legend). Immunohistochemical staining was performed on 4- $\mu$ m paraffin-embedded coronal sections. Anti-BrdUrd labeling was performed as described (19). Anti-IdUrd staining was performed by using the anti-IdUrd monoclonal antibody, IU4 (Caltag, South San Francisco), which reacts with both BrdUrd and IdUrd. For visualization of the IdUrd-positive cells, Vectastain-AP and the alkaline phosphatase substrate kit (Vector Laboratories) were used. Blue cells without horseradish peroxidase signals represented the cells showing positive labeling for IdUrd but not for BrdUrd (Q cells).

**Detection of Apoptosis.** Evaluation of apoptosis was performed in E14.5 4- $\mu$ m paraffin-embedded sections by using Apoptag (Intergen, Purchase, NY).

**Long-Term BrdUrd Labeling of Slowly Dividing Cells.** BrdUrd (1 mg/ml) was given, mixed with drinking water, to 20- to 24-week-old adult *HuD*  $-/-$  mice and their littermates for 4 weeks, followed by a 1-week BrdUrd free-chase period to wash out rapidly dividing

cells. Four-micrometer-thick paraffin-embedded sections were immunostained as described for the embryonic sections. The number of BrdUrd-positive cells was counted in one-half of five independent sections for each frontal level.

**Statistical Analysis.** The statistical significance of differences was analyzed by using Student's *t* test ( $n > 3$ , each group). All values were expressed as mean  $\pm$  SEM. Asterisks on the error bars denote statistical significance ( $P < 0.05$ ).

## Results

**Targeted Disruption of the *HuD* Gene.** Targeted disruption of the *HuD* locus in ES cells was performed and confirmed as described in Fig. 1 A and B. Interbreeding of the heterozygous mutant (*HuD*  $+/-$ ) mice yielded homozygous mutant (*HuD*  $-/-$ ) pups with the expected Mendelian ratio, indicating that HuD may not be essential for embryonic viability. We confirmed the absence of *HuD* mRNA (Fig. 1C) in adult homozygous mouse brains by RT-PCR. To demonstrate the absence of the HuD protein in *HuD*  $-/-$  mice, we performed immunoblotting of brain lysates with anti-HuD-specific monoclonal antibody 16C12 (Fig. 1D Upper Left) and anti-HuB/C/D serum (Fig. 1D Lower Left). Liver lysates of wild-type mice were also characterized with these antibodies as negative controls (see Fig. 1D legend). In *HuD*  $-/-$  mice, the band corresponding to HuD (indicated by the double arrowhead, Fig. 1D Upper Left) was absent in the immunoblot with the anti-HuD antibody. The results of the immunoblot with anti-HuB/C/D serum are shown in Fig. 1D Lower. The level of expression of the band indicated by the single asterisk was not significantly changed in the *HuD*  $-/-$  brain, whereas the expression of the band indicated by the single arrowhead decreased. Taken together, these results show that expression of HuD protein is missing, and expression of HuB/C proteins is unlikely to be strongly affected in *HuD*  $-/-$  mice, although we cannot exclude the possibility of attenuated expression of other splice variants of HuB/HuC by this immunoblot.

**Neural Development and Motor Functions in *HuD*-Deficient Mice.** We first visualized and evaluated the midembryonic nervous system development of *HuD*  $-/-$  animals by using whole-mount immu-

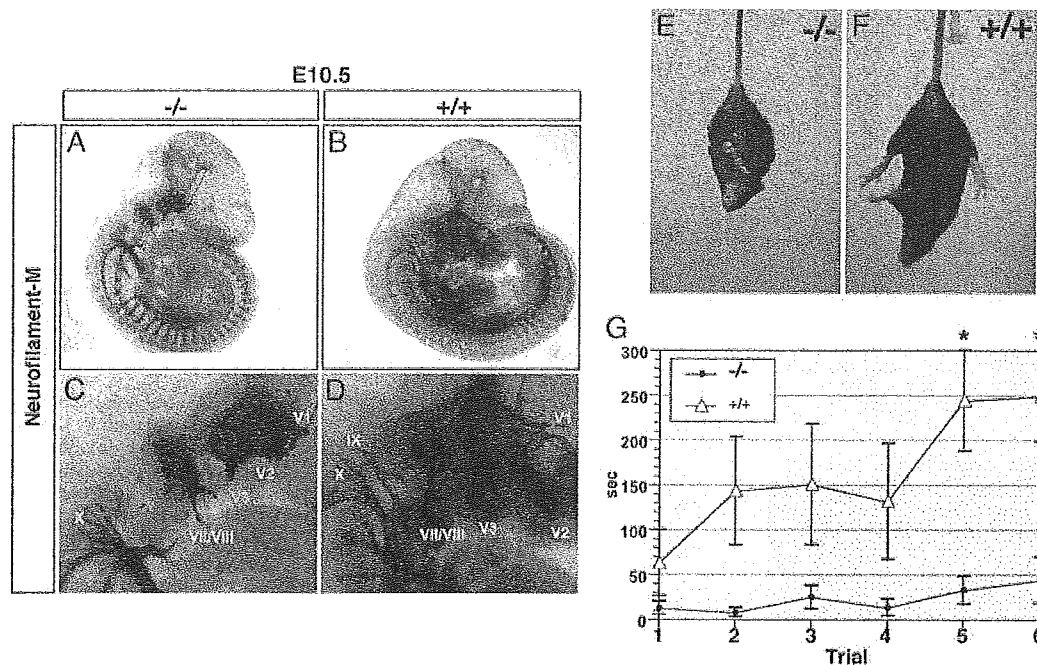


**Fig. 2.** Histological analysis of the *HuD*-deficient mouse embryos. (A–D) Lateral views of E10.5 embryos of *HuD*<sup>-/-</sup> mice (A and C) and their wild-type littermates (B and D) stained with 2H3 antineurofilament-M antibody. In the wild-type embryos, axons of the glossopharyngeal nerve (IX) and hypoglossal nerve (XII) are seen extending from the caudal hindbrain and rostral spinal cord. On the other hand, the axons of these cranial nerves are not visualized in the *HuD*<sup>-/-</sup> embryos. Development of other cranial nerves, including the trigeminal (V) and acousticofacial (VII/VIII) nerves, also seems to be impaired in the *HuD*-deficient embryos as compared with that in their wild-type littermates. (E and F) The hind-feet-clenching phenotype in adult *HuD*<sup>-/-</sup> mice at 24 weeks of age. The *HuD*<sup>-/-</sup> mice displayed hind-feet-clenching behavior when picked up by the tail from 4 to 8 weeks of age (E). In wild-type littermates, however, the angles of the hind feet were close to a right angle (F). (G) Rotarod analysis. *HuD*<sup>-/-</sup> and their wild-type littermates at 20–26 weeks of age were used for the analysis. In *HuD*<sup>-/-</sup> mice, improvement of retention time by learning could scarcely be seen. The retention time was significantly shorter in the *HuD*<sup>-/-</sup> mice than in the wild-type littermates in the fifth and sixth trials.

nostaining of Neurofilament-M at the stage of E10.5, when *HuD*-positive mature neurons normally extend neurites toward the ventral neural tube (Fig. 2A–D). We observed that the neurite extension of several cranial nerves [glossopharyngeal nerve (IX), hypoglossal nerve (XII), trigeminal nerve (V), and acousticofacial (VII/VIII) nerves] was impaired in most *HuD*<sup>-/-</sup> embryos (Fig. 2A and C). However, no such developmental delay of the nervous system was observed in later-stage embryos. In E14 and E16 embryonic sections, the expression of neuroepithelial markers (Nestin or Musashi-1) in the VZ remained undisturbed (data not shown). No morphological abnormalities of the central nervous system were observed in E14 embryos (Fig. 7A and B, which is published as supporting information on the PNAS web site), indicating that the above-mentioned impaired-cranial-nerve-development phenotype appeared only transiently. The apparent masking of the cranial-nerve-phenotype in the later-stage embryos could perhaps be explained by the sequential onset of expression of the other *Hu* proteins in the developing nervous system (4).

*HuD*<sup>-/-</sup> pups were indistinguishable from their wild-type littermates during the first several postnatal weeks, in terms of both their size and appearance. There were no significant differences between adult *HuD*<sup>-/-</sup> mice and their wild-type littermates with respect to the structure of the brain as evaluated by histological analysis. The structures of the cerebral cortex, cerebellum, and hippocampus were indistinguishable between *HuD*<sup>-/-</sup> mice and their wild-type littermates (Fig. 7C–F). Although we could not find any significant morphological abnormalities between the two groups of mice in the adult spinal cord either, including the dorsal root ganglia (data not shown), by 4–8 weeks postnatally, 70–80% of the *HuD*<sup>-/-</sup> animals showed a consistently abnormal clasping reflex of the hind limbs upon being suspended by the tail, whereas

age-matched wild-type animals extended their limbs normally (Fig. 2E and F). This clasping phenotype is seen in mutant mice with cortical (20) and basal ganglia defects (21) and indicates the presence of motor/sensory defects in adult *HuD*-deficient mice. To determine whether *HuD* deficiency affected the sensory and/or motor functions of the mature nervous system, we conducted rotarod analysis to evaluate motor coordination in *HuD*<sup>-/-</sup> adults. (Fig. 2G). Six trials were performed for each individual, and the duration for which the mice could stay on an accelerating rotarod without falling was measured. It was found that the duration for which *HuD*<sup>-/-</sup> mice could stay on the rotarod without falling was significantly shorter than that of their wild-type littermates. When the test was repeated, although the performance of wild-type mice improved significantly after a few trials, *HuD*<sup>-/-</sup> mice continued to perform very poorly even after several trials. In addition, the reproductive performance of the *HuD*<sup>-/-</sup> mice was noted to be poor as compared with that of their wild-type littermates.

**Analysis of the Neuronal Cell Lineage in *HuD*<sup>-/-</sup> Embryos.** We then examined the role of *HuD* in neuronal cell lineage development by using the neurosphere assay, which is a selective culture system for neural stem/progenitor cells (18). The ganglionic eminence or cerebral cortex from E14.5 *HuD*<sup>-/-</sup> embryos, as well as their littermates as controls, was dissociated into single cells and cultured in the presence of EGF and FGF type 2 to generate neurospheres. The number of neurospheres formed under this condition is believed to reflect the number of spheres forming multipotent neural stem cells within the dissociated cell population. As shown in Fig. 3A, the number of primary neurospheres formed from the *HuD*<sup>-/-</sup> embryonic ganglionic eminence was 1.5-fold higher in